PROC. OF JSCE,
No. 278, October 1978

COMPRESSIVE STRENGTH OF PLATES WITH CLOSED-SECTIONAL RIBS

By Yoshikazu YAMADA, Eiichi WATANABE** and Ren ITO****

SYNOPSIS

After a series of famous accidents of box girder bridges in the last decade, extensive and elaborate research programs have been under way at various institutions aiming at establishing more reasonable design code of box girders.

The proper choice and determination of the cross section, layout, and steel for the stiffeners are of great importance for the economical and safe design of stiffened plates.

The interest of the proposed study is specifically focused on the effect of the large torsional rigidity of ribs, which in general practice has been neglected, upon the load carrying capacity of stiffened plates.

The proposed study consists of the experimental work and the theoretical analysis. In the experiment, the longitudinal ribs were made of rectangular tubes, and seven test specimens were subjected to the axial compression by universal testing machine, of which one was an unstiffened plate, three with single longitudinal rib, and three with two longitudinal ribs. The theoretical analysis consists of buckling analyses using finite element method and the Simplified Element Method which one of the authors developed.

The result of the proposed study shows that the effect of the large torsional rigidity of the ribs is quite beneficial as far as the buckling load is concerned; however, this effect upon the ultimate strength was found not so eminent.

1. INTRODUCTION

It is generally believed that large plate structures can be more efficiently designed using proper stiffeners than making the thickness of the plate element thicker. Thus, as a steel structure becomes larger, the thinner the cross section becomes, and the method of reinforcement is of great importance.

Timoshenko[1] made use of Fourier series analysis to obtain the buckling coefficient of stiffened plates in terms of the aspect ratio, relative flexural rigidity, relative cross sectional area of ribs. He made clear that this coefficient can not be made larger once the relative flexural rigidity exceeds certain optimal value. DIN 4114[2] adopted his results and specifies the optimal relative flexural rigidity. Klöppel, Sheer, and Möller[3),4)] examined the buckling coefficients of stiffened plates extensively and came up with a great number of charts. However, all of the study mentioned so far were restricted to the case of having ribs without substantial torsional rigidity.

The effect of the torsional rigidity of the ribs was first studied by Wah.[5] More recently, this effect has been studied by Usami,[6] Hasegawa, Nishino, and Okumura[7),8)], and very lately by Ohmura and Yoshinami.[9]

Usami made use of FSM and considered both St. Venant's torsional rigidity and warping rigidity as well as the residual stress to obtain the inelastic buckling load of stiffened plates with open sectional ribs. On the other hand, Hasegawa et al. made use of finite strip method to perform the buckling analysis considering the above-mentioned rigidities and the polar radius of inertia. They concluded that the effect of the torsional rigidity upon the buckling strength is quite significant. Furthermore, Ohmura and Yoshinami made use of orthotropic plate theory of order 8, and concluded that the effect of the torsional rigidity of ribs is strongly influenced by the aspect ratio of the stiffened plates.

The present paper is concerned with this torsional effect upon the buckling load, and to be more important, the load carrying capacity of

* Dr. Eng., Professor, Kyoto University.
** Ph. D., Associate Professor, Kyoto University.
*** M. S., Kohnoike-gumi Construction Company.

stiffened compressed plates.

2. EXPERIMENTAL INVESTIGATION

(1) Description of Test

The general description of the test program will be briefly given in the following manner.

Cross sectional properties **Fig. 1** shows the cross section of the longitudinal ribs. Test specimens are named Case i (i=0, 1, 2, ..., 6): Case 0 refers to the unstiffened plate, Cases 1 to 3 refer to the cases with single longitudinal rib, and Cases 4 to 6 refer to the cases with two longitudinal ribs. The ribs are designed in such a way that for each Case i (i=1, ..., 6), they possess just about the optimal flexural rigidity γ^*. Their geometric dimensions are shown in **Table 1**.

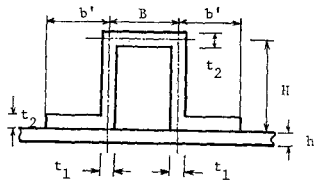

Fig. 1. Cross Section of a Rib.

Table 1 Cross Sectional Dimensions of Ribs. Cases 1 to 6 (in mm)

Case No.	B	H	b'	h	t_1	t_2
1	52.4	14.6	15.8	3.2	3.4	3.2
2	23.1	19.1	15.1	3.2	3.4	3.2
3	14.5	21.9	15.2	3.2	3.4	3.2
4	33.4	21.6	15.0	3.2	3.4	3.2
5	19.5	25.1	15.1	3.2	3.4	3.2
6	13.0	28.3	15.0	3.2	3.4	3.2

The effect of the constraint on warping is deemed small as compared with that of St. Venant torsion in the case of closed cross section and thus, the torsional warping rigidity was not taken into account. The slenderness ratio of the panel was so determined that the testing could be performed using relatively small testing machine of capacity fifty tons.

The torsional rigidity of the rib is expressed by $\eta=GJ_s/EI_s$, which is the ratio of St. Venant's torsional rigidity to the flexural rigidity of a rib. In **Table 2**, the basic four parameters are given by the following equations:**

** EI_s=flexural rigidity, GJ_s=torsional rigidity of a rib. D=flexural rigidity of isotropic plates.

Table 2 Cross Sectional Dimensions and Properties of Test Specimens.

Case No.	N	a (mm)	b (mm)	t (mm)	A_s (cm²)	I_s (cm⁴)	J_s (cm⁴)	δ	γ	η	γ^*
0	0	900	800	3.2	—	—	—	—	—	—	—
1	1	900	800	3.2	2.82	3.49	1.11	0.110	14.53	0.123	10.9
2	1	900	800	3.2	2.99	3.38	2.22	0.114	14.10	0.252	11.0
3	1	900	800	3.2	3.53	3.35	4.23	0.138	13.96	0.485	11.5
4	2	900	800	3.2	3.19	6.63	1.20	0.124	27.62	0.070	20.0
5	2	900	800	3.2	3.19	6.00	2.43	0.124	25.00	0.156	19.9
6	2	900	800	3.2	3.39	5.93	4.76	0.133	24.70	0.308	20.3

$$\delta=A_s/(bh);\quad \gamma=EI_s/(bD);\quad \eta=GJ_s/(EI_s) \qquad \cdots\cdots(1)$$

and

$$\gamma^*=\alpha^2\{8(1+2\delta)-1\}-\alpha^4/2+(1+2\delta)/2 \quad \text{for } N=1$$

where $\alpha<\sqrt{8(1+2\delta)-1}$ $\qquad \cdots\cdots(2)$

$$\gamma^*=\alpha^2\{12(1+3\delta)-2/3\}-\alpha^4/3+(1+3\delta)/3 \quad \text{for } N=2$$

where $\alpha<\sqrt{18(1+3\delta)-1}$ $\qquad \cdots\cdots(3)$

The hollow ribs were made by cutting from the rectangular bars. These are fastened to the flange plate by taps.

Shape of the panel and support condition The plate thickness is kept to be 3.2 mm, and the aspect ratio of the panel is also kept constant to

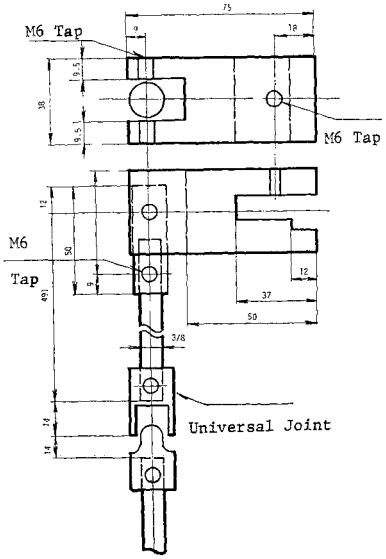

Fig. 2 Rig for Simply Supported Edges.

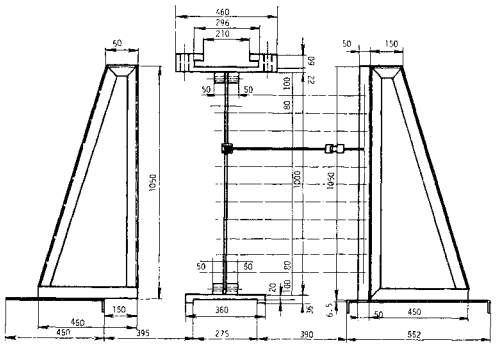

Fig. 3 Test Setup.

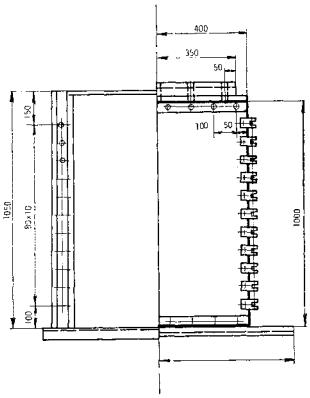

Fig. 4 Tested Panel.

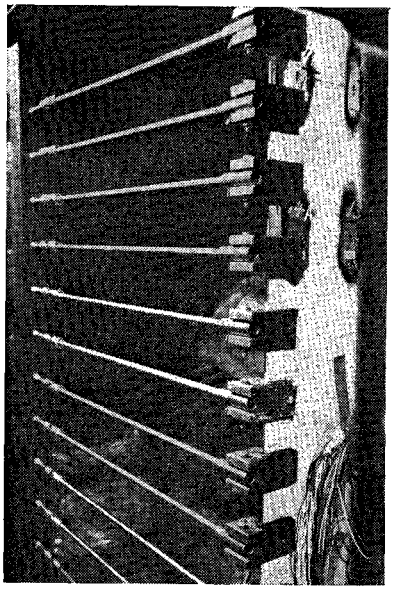

Photo 1 Rig for Simply Supported Edges.

Table 3 Results of Standard Testing (In accordance with JIS, Japanese Industrial Standards). Number of Specimens=12. Material: SS41

	Mean Value (kg/cm^2)	Standard Deviation (kg/cm^2)
Yielding Strength σ_Y	2442	34
Ultimate Strength σ_u	3517	41

be 1.125. The support condition was determined considering the easiness of loading and fabrication of the specimens. Thus, the supporting frames were designed in such a way that the loaded edges are clamped and the unloaded edges simply supported with respect to the out-ot-plane deflection of the panel. For the fulfilment of the simply supported edges, rig such as shown in **Fig. 2** and **Photo 1** was used. The supporting frames are shown in **Fig. 3**. One is for the attachment of displacement transducers, and the other is to receive the reaction force from the simply supported edges of the specimens, and hence firmly anchored to the concrete bed. On the other hand, the clamped edges are provided using steel rectangular bars as can be seen from **Figs. 3** and **4**.

As can be noted, from **Fig. 2**, there existed an undesirable discrepancy between the theoretical and the actual panel width designated by "b", as far as out-of-plane displacement is concerned.

It must also be mentioned that the rig employed herein finds its very origin in that conceived by Fukumoto and Usami.[10]

Standard material testing The standard testing was conducted to obtain the yielding strength of steel plates of thickness 3.2 mm. The result is shown in **Table 3** (Universal testing machine REH-100TV was used).

Calibration of testing machine The axial compression tests were conducted using Amsuler testing machine of capacity 50 tons. From the structure of the machine and the nature of the testing, it was not possible to use load cells during testing. Thus, it was necessary to conduct the calibration test beforehand. A good linear relationship was confirmed to exist between the reading of the machine, P_{AM} and that of the load cell, P_{LC}.

Compression tests of stiffened plates Seven test specimens, Cases 0 to 6 were tested until failure. After a test specimen was set using plummet, the initial out-of-plane displacements were measured using transit and stainless steel scale. During the testing, the following readings were recorded:

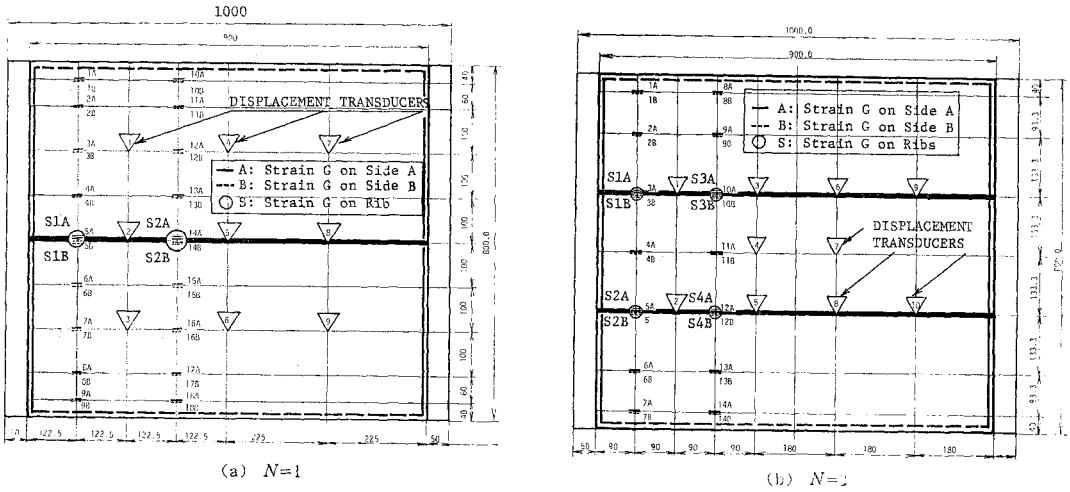

(a) $N=1$ (b) $N=3$

Fig. 5 Instrumentation.

of testing machine, displacements of grid points, and the strains of the specimens. The instrumentation is shown in **Fig. 5**. The positions of instrumentation were determined in accordance with the mesh points of both FEM and SEM, Simplified Element Method, analysis.

(2) Evaluation of Plate and Rib Stresses

Strains were measured for i) investigating the general behavior of stiffened plates, ii) investigating the load distribution characteristics of ribs in relation to the plate element, and iii) checking the reliability of experimental data. The last purpose points out the necessary condition that the total load from the testing machine must be equilibrated by the total longitudinal reaction force of the stiffened plate.

Assuming the linear elasticity of the material, the average axial stress of the stiffened plate panel can be given by the equation

$$\sigma_x = E\frac{\epsilon_A+\epsilon_B}{2} \quad \cdots\cdots(4)^*$$

where, the transverse stresses are assumed to be negligible, and ϵ_A and ϵ_B refer to the measured strain on surface A and B, respectively as shown in **Fig. 5**. Let the total axial force exerted on the plate element be designated by P_p, then the equilibrium requires that

$$P_p = \int \sigma_x dA \quad \cdots\cdots(5)$$

Similarly, let P_s designate the axial force carried by the rib(s), then it can be obtained from the strains of ribs as explained by **Fig. 6**:

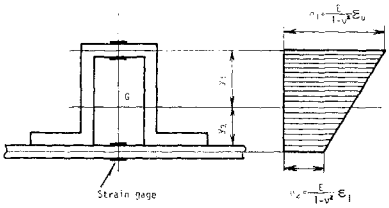

Fig. 6 Axial Strain Distribution of Ribs.

$$P_s = \frac{A_s E}{1-\nu^2}\frac{y_2\epsilon_u + y_1\epsilon_l}{y_1+y_2} \quad \cdots\cdots(6)$$

Now, let's define a reliability index R by the following equation:

$$R=(P_p+P_s)/P_{LC}\times 100(\%) \quad \cdots\cdots(7)$$

If loads P_p, P_s, and P_{LC} were true ones, then R should not differ from 100%; however, actually, this is not the case since i) the transverse average stress σ_y is neglected, ii) formula for P_s ceases to be valid in the elasto-plastic range, and iii) the strain distribution shown in **Fig. 6** is only the first approximation. However R value may show the general consistency of P_{LC} measured by the testing machine, and P_p+P_s measured by the electric strain gages.

3. THEORETICAL INVESTIGATION

(1) Formulation by Means of SEM[11)~13)]

SEM is an abbreviation of Simplified Element Method that has been developed by one of the

* plane stress state is assumed.

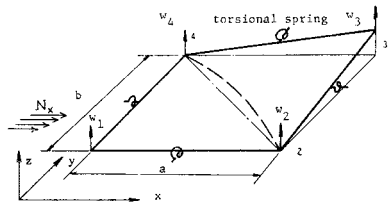

Fig. 7 Shape Function in Simplified Element Method.

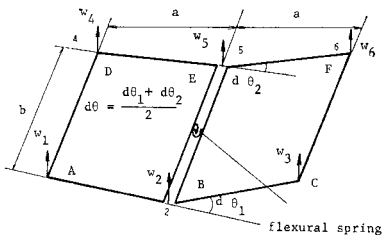

Fig. 8 Flexural Spring.

authors.* This method utilizes incompatible shape functions for the out-of-plane displacement to reduce the element's degree-of-freedom. In order to make up for the incompatibility of shape functions SEM installs both flexural and torsional springs.

Brief explanations will be given on SEM in the following.

Strain energy of element Using the coordinates in **Fig. 7**, the strain energy U_e of an isotropic plate element can be given by the equations:

$$\left.\begin{aligned} &U_e=U_{1e}+U_{2e}+U_{3e} \\ &\text{where} \\ &U_{1e}=\frac{D}{2}\int_0^a\int_0^b\{(w,_{xx})^2+(w,_{yy})^2\}\,dxdy \\ &U_{2e}=\frac{D}{2}\int_0^a\int_0^b\{2(w,_{xy})^2\}\,dxdy \\ &U_{3e}=\frac{D}{2}\int_0^a\int_0^b\{2\nu[w,_{xx}w,_{yy}-(w,_{xy})^2]\}\,dxdy \end{aligned}\right\} \quad \cdots\cdots(8)$$

where $w,_{xx}$, $w,_{yy}$, and $w,_{xy}$ refer to the second order partial derivatives of the deflection, w.

Shape function The deflection is assumed in the following hyperbolic paraboloid surface:

$$w=a_1+a_2x+a_3y+a_4xy \quad \cdots\cdots(9)$$

where the constants a_i(i=1, ..., 4) can be determined in terms of nodal displacements w_i (i=1,..., 4):

$$\left.\begin{aligned} &a_1=w_1;\quad a_2=(w_2-w_1)/a;\quad a_3=(w_4-w_1)/b; \\ &a_4=(w_1-w_2+w_3-w_4)/(ab) \end{aligned}\right\} \quad \cdots\cdots(10)$$

Fig. 8 shows two adjacent plate panels joined by a flexible spring. The spring represents the average flexibility corresponding to the bending action to make up for the inconsistency introduced by the above shape function. The bending moment per unit length, m_x, acting perpendicular to the boundary line BE is approximated by the equation:

$$\left.\begin{aligned} &m_x=D(w,_{xx}+\nu w,_{yy})\cong Dw,_{xx}=D(\theta_x),_x \\ &\quad=k'_{bx}d\theta_x \\ &\text{where} \\ &k'_{bx}=D/a;\quad d\theta_x=(w_1-2w_2+w_3+w_4-2w_5 \\ &\qquad\qquad +w_6)/(2a) \end{aligned}\right\} \quad \cdots\cdots(11)$$

Therefore the total bending moment, M_x is given by the equations:

$$M_x=k_{bx}d\theta_x;\quad k_{bx}=Db/a=D/\alpha;\quad \alpha=a/b \quad \cdots\cdots(12)$$

Similarly for the transverse direction, the bending moment M_y can be given by:

$$M_y=k_{by}d\theta_y;\quad k_{by}=D\alpha \quad \cdots\cdots(13)$$

Thus, the strain energy U_{1e} can be well approximated by:

$$U_{1e}=\frac{k_{bx}}{2}(d\theta_x)^2+\frac{k_{by}}{2}(d\theta_y)^2 \cdots\cdots(14)$$

The strain energy resulting from the torsional deformation can be obtained by substituting the shape function into the expression of U_{2e} referring to **Fig. 7**.

$$\begin{aligned} U_{2e}&=Dab(a_4)^2=4\times\frac{1}{2}\left(\frac{D}{2}\right)ab(a_4)^2 \\ &=4\times\frac{1}{2}k^*_{tp}ab(a_4)^2 \end{aligned} \quad \cdots\cdots(15)$$

The evaluation of the strain energy U_{3e} is not so easy. However, from the calculus of variations[1)]

---

* Similar method has been proposed by Kawai[14)] called Rigid Bodies-Spring Models. However, this is quite different from SEM in two respects: one in the shape function, and another in the shape of element.

* k_{tp} refers to the spring constant of the equivalent torsional spring. (=$D/2$). However, the use of this constant is not mandatory in this study.

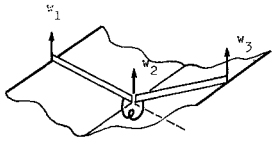

Fig. 9 Bending of Rib.

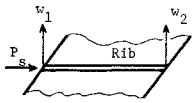

Fig. 10 Work of Rib.

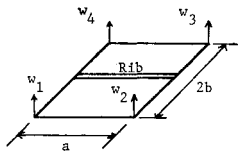

Fig. 11 Torsion of Rib.

this term is known to vanish in the case of edges simply supported or clamped. In the proposed study, the boundary condition is such that the loaded edges are clamped and unloaded edges simply supported, thus SEM may be thought applicable to the proposed study.

The strain energy due to the flexural deformation of ribs can be given by*:

$$U_{bs}=\frac{1}{2}\frac{EI_s}{a}\theta_s^2;\quad \theta_s=(w_1-2w_2+w_3)/a$$

(see **Fig. 9**) .....(16)

The work done by the plate element due to the action of axial thrust N_x is given by the equation: (See **Fig. 7**)

$$W_x=\frac{N_x}{2}\int_0^a\int_0^b (w,_x)^2 dxdy \quad .....(17)$$

The work done by the axial rib force P_s through the flexural deformation of the rib is given by the equation: (See **Fig. 10**)

$$W_s=\frac{P_s}{2}\int_0^a (w,_x)^2 dx \quad .....(18)$$

Finally, the strain energy due to the torsional deformation of ribs can be given by the equation: (See **Fig. 11**)

$$U_{ts}=\frac{1}{2}\frac{GJ_s}{a}\phi_s^2;\quad \phi_s=(w_4-w_2+w_1-w_3)/(2b)$$

.....(19)

Buckling analysis by SEM From the foregoing representation of the strain energy and work, the equations of equilibrium can be derived by use of the principle of virtual displacement:

$$[K]\{w\}=\lambda[K_G]\{w\} \quad .....(20)$$

where $\{w\}$ refers to the total degree of freedom of the out-of-plane displacement of the stiffened plate, and

$$\left.\begin{aligned}&\lambda=N_x a^2/D;\quad [K_G]=[K_{Gp}]/6+n\delta[K_{Gs}]\\&[K]=[K_{bpx}]+n\gamma[K_{bs}]+\alpha^4[K_{bpy}]\\&\qquad+\alpha^2(1-\nu)(2[K_{tp}]+\eta[K_{ts}])\end{aligned}\right\} \quad .....(21)$$

in which the subscripts p, s, b and t refer to the plate element, stiffener, flexure, and torsion, respectively, and

a=length of a SEM element; n=number of transverse meshes, furthermore, the above matrices can be obtained by globalization of the element stiffness matrices: (upperscript e refers to the element stiffness)

$$\left.\begin{aligned}&[K^e_{bpx}]=[K^e_{bpy}]=\frac{1}{8}\begin{bmatrix}2&&&&&\\-4&8&\text{sym.}&&&\\2&-4&2&&&\\2&-4&2&2&&\\-4&8&-4&-4&8&\\2&-4&2&2&-4&2\end{bmatrix}\\&\qquad\text{(See \textbf{Fig. 8});}\\&[K^e_{bs}]=\begin{bmatrix}1&-2&1\\-2&4&-2\\1&-2&1\end{bmatrix}\ \text{(See \textbf{Fig. 9});}\\&[K^e_{tp}]=\begin{bmatrix}1&&\\-1&1&\text{sym.}\\1&-1&1\\-1&1&-1&1\end{bmatrix}=[K^e_{ts}]\ \text{(See \textbf{Fig. 7} and \textbf{Fig. 11});}\\&[K^e_{Gp}]=\begin{bmatrix}2&&\\-2&2&\text{sym.}\\-1&1&2\\1&-1&-2&2\end{bmatrix}\ \text{(See \textbf{Fig. 7});}\\&[K^e_{Gs}]=\begin{bmatrix}1&-1\\-1&1\end{bmatrix}\ \text{(See \textbf{Fig. 10})}\end{aligned}\right\}$$

.....(22)

(2) Formulation by Means of FEM

The buckling load of the stiffened plates was

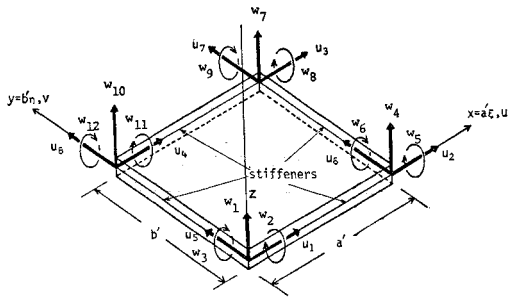

Fig. 12 Finite Element of Stiffened Panel.

* Ribs are assumed to be replaced by idealized symmetrically fastened ones to the plate element.

obtained initially by finite element with the rectangular element shown in **Fig. 12**. This element is an ACM element characterized by the nonconforming cubic shape function and the rectangular element. The exact formulation of the problem is performed in Reference[15], thus, the formulation is entirely omitted herein.

(3) Accuracy of SEM

Several examples will be shown to show the relative error to the exact solution and the out-of-plane degree-of-freedom.

Buckling load of compressed simply supported square plate[1),18)]

	FEM (ACM)	SEM			
partition	4×4	3×3	4×4	5×5	6×6
rel. error (%)	−5.89	−4.25	−2.86	−2.06	−1.55
out-of-plane D.O.F.	39	4	9	16	25

This example demonstrates the validity of SEM.

Buckling load of simply supported square plate under pure shear[1),18)]

	FEM (ACM)	SEM			
partition	4×4	3×3	4×4	5×5	6×6
rel. error (%)	−10.71	73.28	22.18	10.32	5.80
out-of-plane D.O.F.	39	4	9	16	25

This example also demonstrates the efficiency of SEM.

Buckling load of compressed plates with a single stiffener[1),12)]

In this example the partition is taken to be 10 × 10 (D.O.F.=81) using SEM model only.

aspect ratio	1	1	1	1	2	2
γ	5	10	5	10	5	10
δ	0.05	0.05	0.1	0.1	0.1	0.1
relative error (%)	1.10	−1.58	−1.55	−1.58	−0.28	0.27

Thus, it may be observed that this method is a reliable method in obtaining the buckling load.

(4) Effect of Torsional Rigidity of Ribs on the Buckling Load

The ribs are designed so that $\gamma=\gamma^*$ according to DIN 4114. However, this γ^* value is obtained assuming all edges simply supported. It is thus easily seen that this optimum value may be reduced considering the actual support condition of loaded edges clamped and unloaded edges simply supported. Since the torsional behaviour of the stiffened plates is deeply related to the flexural rigidity, the actual optimal flexural rigidity will be explained in the following section, and then afterwards, the torsional effect will be explained.

Actual optimal flexural rigidity The effect of

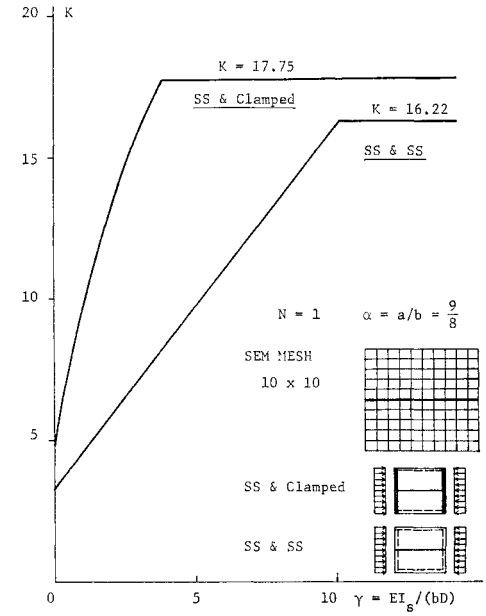

Fig. 13 Buckling Coefficient K and Relative Flexural Rigidity γ of a Rib. Case of a Single Rib.

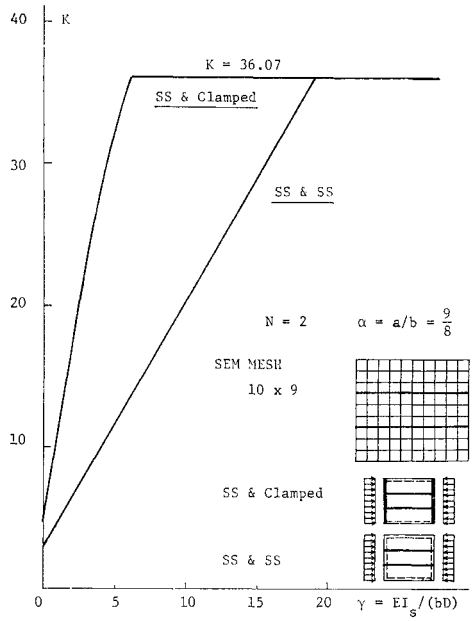

Fig. 14 Buckling Coefficient K and Relative Flexural Rigidity of a Rib. Case of Two Ribs with Equal Spacing.

the rib's flexural rigidity upon the buckling load of stiffened plate is obtained by means of SEM, and is shown in **Figs. 13** and **14**. The torsional rigidity is assumed to be negligible, and the ordinate of these figures refers to the buckling coefficient:

$$k=\sigma_{xcr}/\sigma_E;\quad \sigma_E=\pi^2 D/(b^2 h)=\text{Euler's plate buckling stress.} \qquad \cdots\cdots(23)$$

From these figures, γ^{**}, that is, the actual optimal flexural rigidity can be obtained both for $N=1$ and $N=2$. In the case of $N=1$, $\gamma^*=10$, and γ^{**} turns out to be nearly 4, which is 40% of γ^*. In the case of $N=2$, $\gamma^*=20$, and $\gamma^{**}=6$, which is 30% of γ^*.

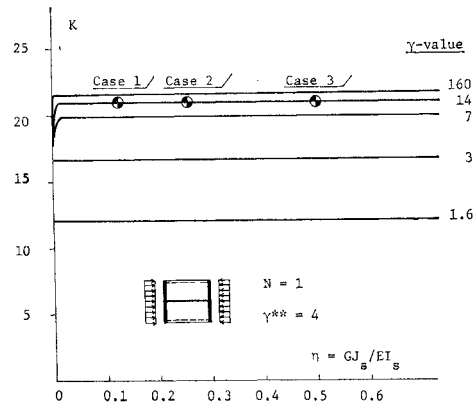

Fig. 15 Effect of Torsional Rigidity of a Rib on Buckling Coefficient. $N=1$.

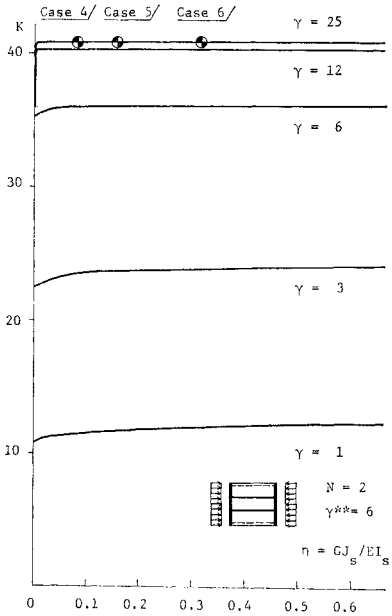

Fig. 16 Effect of Torsional Rigidity of Ribs on Buckling Coefficient. $N=2$.

Buckling load of stiffened plates with torsionally stiff ribs The effect of the torsional rigidity of ribs is analysed using SEM, and the results are given in **Figs. 15** and **16**. In the analysis the value of γ is changed stepwise up to γ^*, or more. The following interpretations can be made from the results:

Case when $\gamma>\gamma^{**}$ When the flexural rigidity of ribs is greater than the optimal value, then higher torsional rigidity is seen to lead to higher buckling coefficient in general. In both cases of $N=1$ and 2, the increment of the buckling coefficient due to the increment of the torsional rigidity takes place within the initial narrow range of $\eta=0\sim0.01$. When the value of η exceeds 0.01, the coefficient remains unchanged. Furthermore, it will be seen that this value of the coefficient depends on the value of γ. Thus, it may be seen that the important thing is whether the torsional rigidity exists or not: If there is some torsional rigidity, then virtually this is the case, the full benefit of torsional rigidity can be expected up to the level of K shown in **Fig. 17**. It will be seen that the increment of the buckling coefficient due to the existence of torsional rigidity is maximum 13% for $N=2$, and 20% for $N=1$.

Case when $\gamma<\gamma^{**}$ When the flexural rigidity of ribs is less than the optimal value, the torsional rigidity does not play any significant role as can be seen from **Fig. 17**.

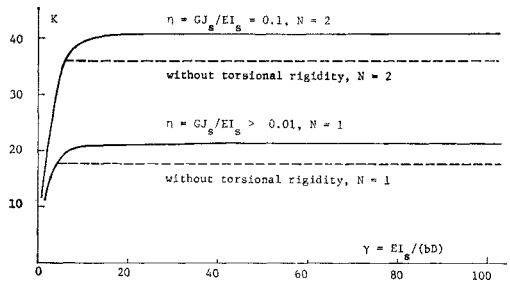

Fig. 17 Effect of Torsional Rigidity Upon Buckling Coefficient.

(5) Evaluation of Buckling Loads of Test Specimens by FEM and SEM

The predicted linear buckling loads are shown in **Table 4**, together with the ultimate loads obtained experimentally. The buckling modes are

Table 4 Buckling Loads of Test Specimens by FEM and SEM, P_{cr} and Experimental Ultimate Load, P_u (in tons).

Case No.	SIMPLIFIED ELEMENT METHOD partition			FEM partition		EXP P_u
	6×6* [25]**	10×10 [81]	12×12 [121]	4×4 [33]	8×8 [161]	
0	4.49	4.65	4.66***	4.41	4.63	8.5
1	15.08	18.15	19.05	17.26	18.84	16.9
2	15.15	18.23	19.12	18.35	19.53	16.0
3	15.51	18.67	19.53	20.09	20.60	16.5

Case No.	SIMPLIFIED ELEMENT METHOD				FEM 5×3 [32]	EXP P_u
	6×6* [25]**	9×9 [64]	10×9 [72]	12×12 [121]		
4	29.76	38.02	39.56	38.69	33.41	34.4
5	29.81	38.07	39.62	38.69	34.29	30.6
6	30.21	38.63	40.19	39.00	35.27	26.4

* $m\times n$ refers to the partition of m intervals in longitudinal and n intervals in transverse directions, respectively.
** figures in bracket show the out-of-plane degree-of-freedom.
*** concides with exact solution.

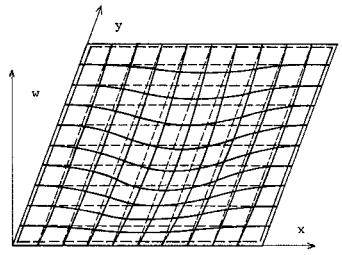

Fig. 18 Buckling Configuration. Case 0.

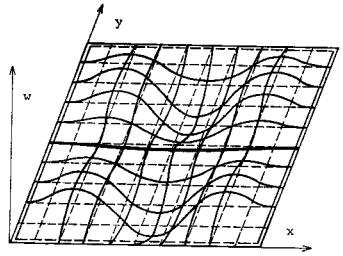

Fig. 19 Buckling Configuration. Cases1–3.

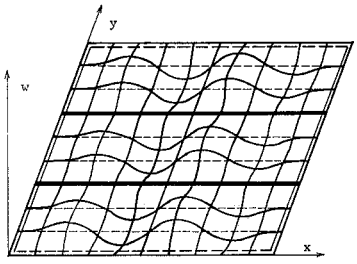

Fig. 20 Buckling Configuration. Cases 4–6.

shown in **Figs. 18, 19** and **20**, for $N=0$, 1, and 2, respectively (by 10×10 & 10×9 model). The results from using 12×12 SEM model may be thought to be very close to the exact values.

(6) Prediction of Ultimate Loads

The ultimate loads may be predicted by Watanabe's formula:

$$\left.\begin{aligned}\frac{P_u}{\sigma_Y bh}&=\sqrt{1+2N\Phi}\,\frac{1.69}{B}\\&\quad+\frac{\Phi}{1+\Phi}\sqrt{N\gamma/\gamma^*}\qquad(N\gamma/\gamma^*\leqq1)\\ \text{where}\quad B&=b/h\sqrt{\sigma_Y/E}:\ \text{generalized slenderness ratio of unstiffened plate}\\ \Phi&=r_sN\delta;\ r_s=\text{yielding strength of rib/that of plate element}\end{aligned}\right\}\quad\cdots\cdots(24)$$

It has been shown that good correlations exist between the results from this formula and various experimental results available.[15]

The ultimate loads of the tested panels as predicted by Eq. (24) are provided in **Table 5**. According to the table, the formula tends to overestimate the strength of most test panels to some extent; however, the correlation will be not too bad.

Table 5 Prediction of Ultimate Loads by Empirical Formula: P_{EM} (tons)

	TEST SPECIMENS						
	Case 0	Case 1	Case 2	Case 3	Case 4	Case 5	Case 6
N	0	1	1	1	2	2	2
P_{EM}	12.4	19.9	20.1	21.3	29.9	29.9	30.9
P_u^{ex}	8.5	16.9	16.0	16.5	34.4	30.6	26.4

4. RESULTS OF COMPRESSION TESTS

(1) Initial Deflection

The results of the measurement of the initial deflections of the tested plates are shown in **Fig. 21**. It seems that the cylindrical surface of the initial deflection was inevitable in view of the fabrication of the test specimens and the structure of the test rig, although the eccentricity of loading was carefully minimized.

(2) Load and Out-of-plane Deflection

Figs. 22 shows the deflections plotted against the jack loads. The deflections are numbered in accordance with **Fig. 5**. From these curves it will be seen that the deflections increased signifi-

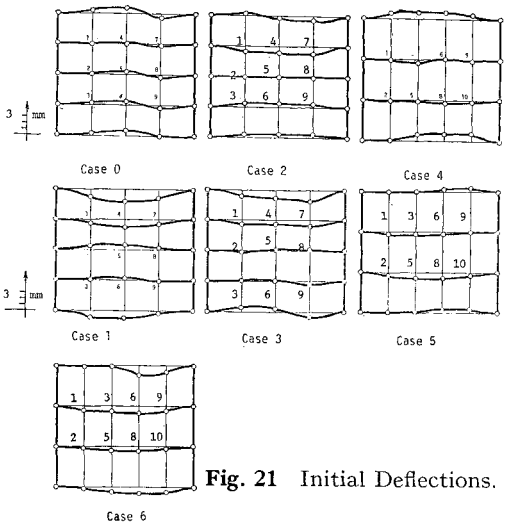

Fig. 21 Initial Deflections.

cantly as the load approached the ultimate value. This phenomenon seems to resemble to those of structures controlled by unstable symmetric bifurcation buckling where the ultimate strength is characterized by outstandingly increasing deflection.

Furthermore, it is to be noted that the ribs underwent significant deflection although the buckling mode of the idealized stiffened plates were such that the ribs formed nodal lines. This difference may be attributed to the assumption that the stiffeners are replaced by the equivalent ones fastened symmetrically to the plate element in the theoretical analysis, in spite of the fact that the actual stiffeners were fastened asymmetrically.

(3) Distribution of Average Axial Strains versus Load

Figs. 23 shows the distribution of the average

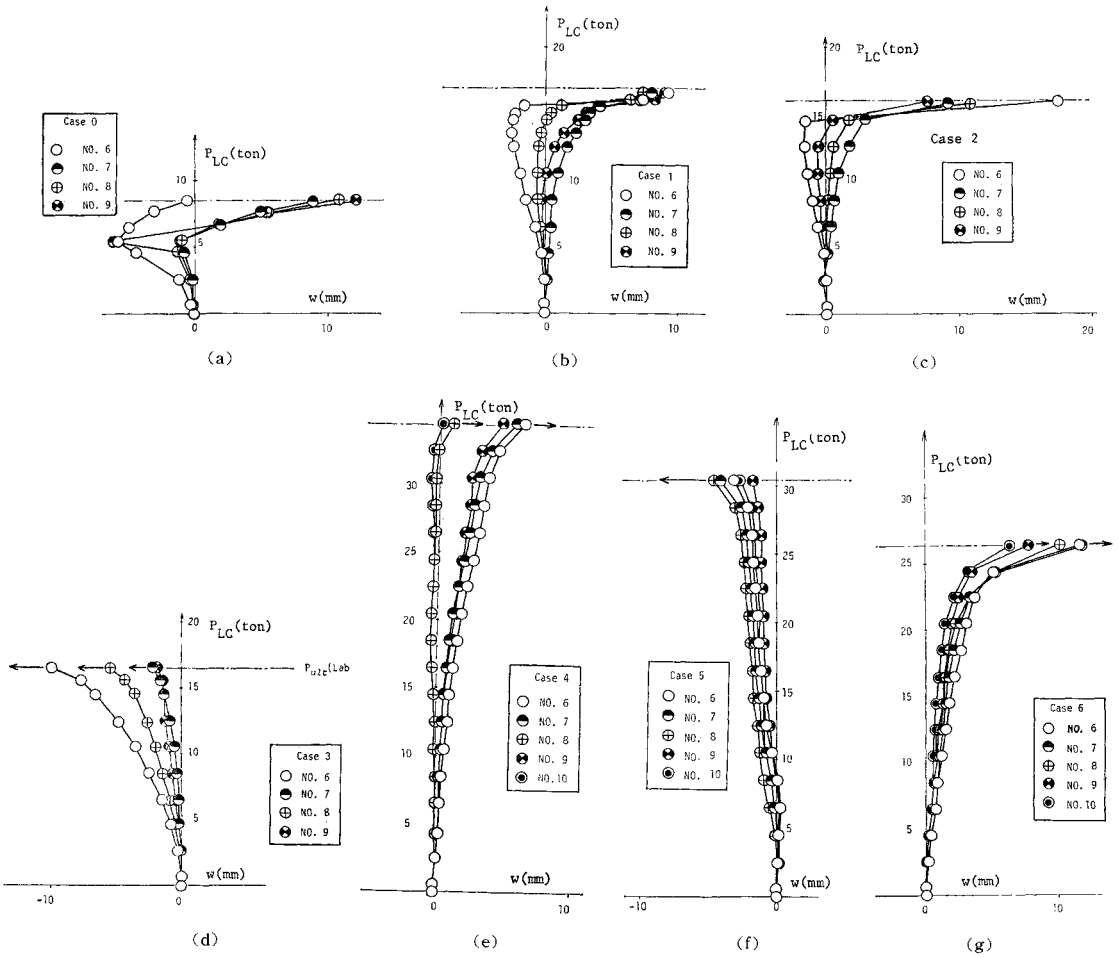

Fig. 22 Load-deflection Curves.

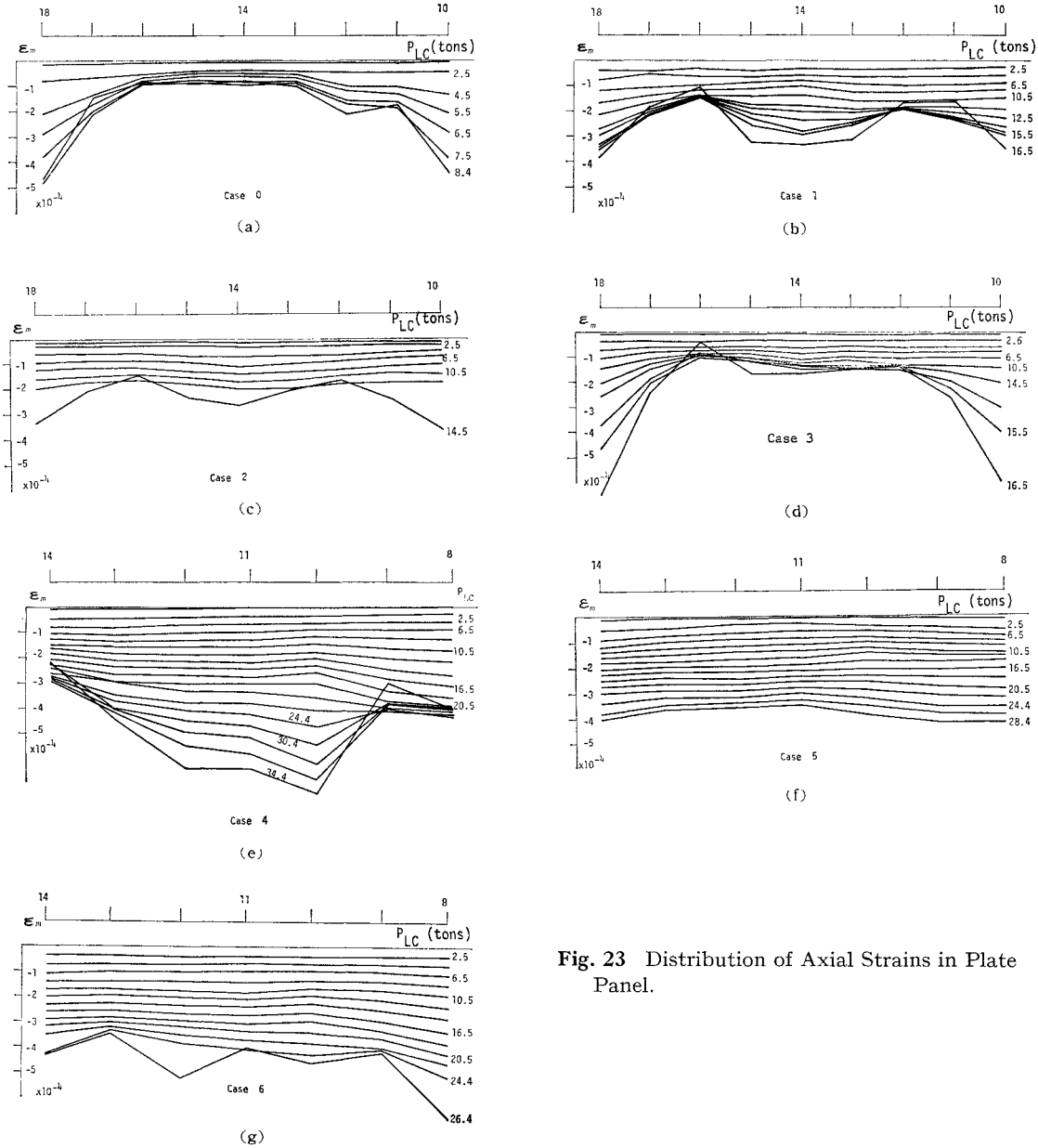

Fig. 23 Distribution of Axial Strains in Plate Panel.

axial strains of test panels for different levels of loading (See also **Fig. 5**).

The axial strain redistributions caused by large deflection of the stiffened plates were found not unique: The distribution in Cases 0 and 3 showed a typical pocket of half wave near the center. Those of Cases 1 and 2 showed strain concentrations along the rib, and showed adjacent pockets. Those of Case 4, on the other hand, showed global convex distribution of axial compressive strains. Moreover, those of Cases 5 and 6 showed rather uniform distributions.

(4) Distribution of Axial Strains of Ribs Versus Load

Figs. 24 shows the distribution of the axial strains of the ribs for different load levels. It will be seen that the failure of the test specimens was

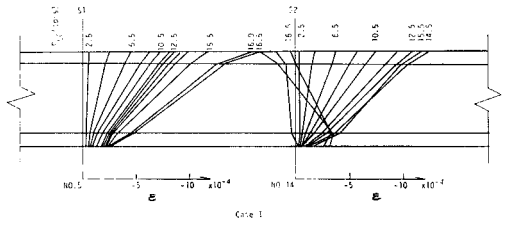

(a) Case 1

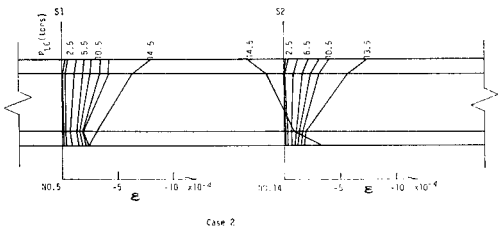

(b) Case 2

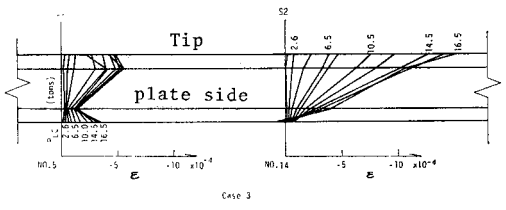

(c) Case 3

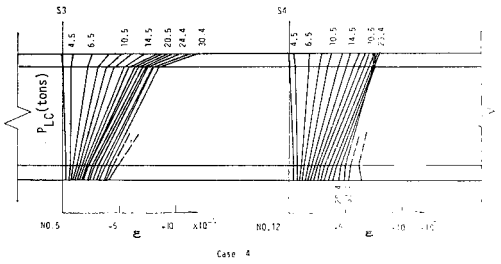

(d) Case 4

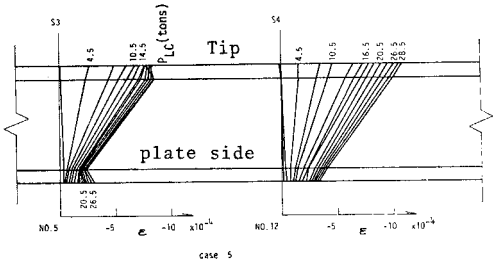

(e) Case 5

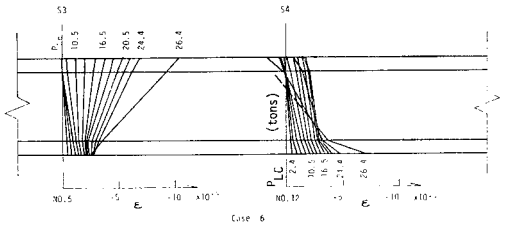

(f) Case 6

Fig. 24 Distribution of Axial Strains of Rib.

accompanied by the plastification of the stiffeners (see **Fig. 5** for the numbering of the ribs).

(5) Load Distribution of Ribs

Figs. 25 shows how the axial load is distributed to the plate and ribs, and the correlation of the load indicated by the testing machine and the one predicted by the strain gages.

Approximately 20–40% of the load was carried by a rib in the case of plates with single stiffener,

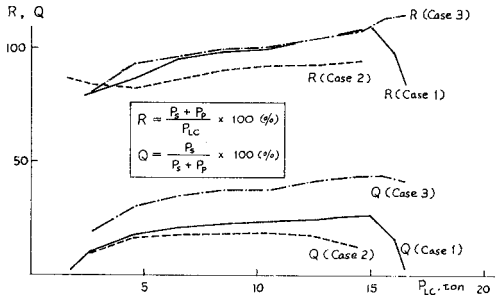

(a) R and Load Distribution Factor, Q. Case 1~3

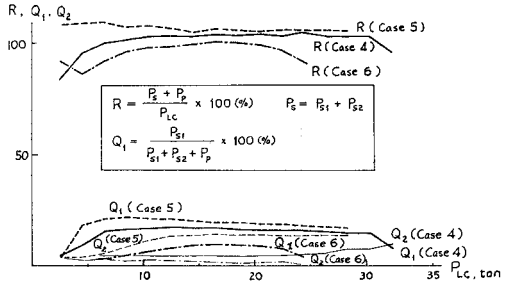

(b) R and Load Distribution Factors, Q_1 & Q_2.

Fig. 25 Reliability Index.

and 10–35% of the load was carried by both ribs in the case of plates with two stiffeners. Among the ribs fastened to the plate elements, those of Case 6 were fabricated in such a way that the ends of the ribs did not touch the loading head. This fact may have resulted in smaller ultimate strength of Case 6 as compared with those of Cases 4 and 5.

The correlation factor R, which was intended to make up for the insufficient information due to not using Rosett gages varied approximately between 80–110%. This value will be seen to have stayed near 100% in the intermediate stage of loading.

(6) Failure Mechanism of Test Specimens

Photo 2 shows Case 1 after the failure. The panel is seen bent plastically near the center. Furthermore, sketches of the failure mechanism of the test specimens are provided in **Fig. 26**. These mechanisms will be seen wholly different from those observed previously[15], where the tested sections were designed to be the compression flange of box girders subjected to two-point loading. That is, in the previous testing, the plastic deformation developed so well that the typical roof-like fold lines were formed. It seems perhaps that this time the supporting frames were not rigid enough against the outstanding growth of the deflections so that the plastic fold lines could not develope well.

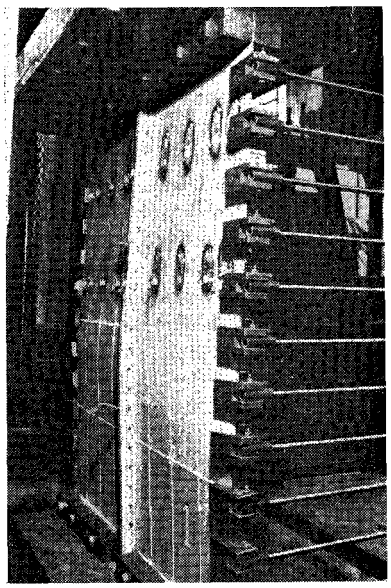

Photo 2 Failure of Test Specimen Case 1. $N=1$.

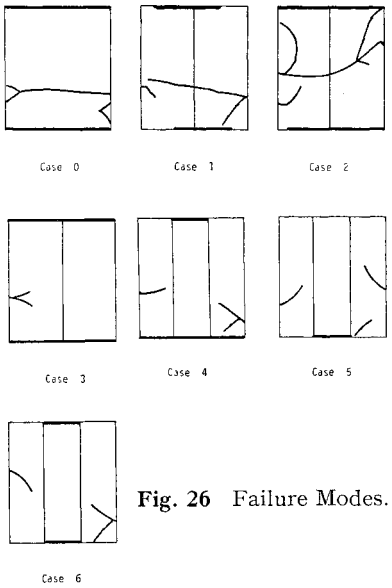

Fig. 26 Failure Modes.

5. DISCUSSIONS

Before the test program was completed, the authors believed for sure that the ultimate strength of plates under compression could be greatly increased by using closed-sectional ribs. However, the results have shown that this is not always true.

Compared with the last experimental program, the test specimens were independent plates. This made it easy to fabricate the specimens and to perform the test; however, this setup proved to be insufficient for the purpose of observing the absolutely ultimate behaviour of stiffened plates of box girders.

The accuracy of the proposed method named SEM, Simplified Element Method was proved good enough in the buckling analysis of plate structures.

As mentioned earlier, the tested panels were designed and fabricated so that the testing could be performed using relatively small loading machine; moreover, the cross sectional parameters may have differed from those currently adopted in usual engineering practice.

6. CONCLUSIONS

This study is concerned with the strength of compressed plates stiffened longitudinally with ribs of closed cross section. From both experi-

mental and theoretical investigations, the following conclusions may be drawn:

(1) The buckling strength of stiffened plates can be significantly improved by the existence of torsional rigidity up to certain maximum value in the case when the flexural rigidity of the rib is more than the optimal value; however,

(2) the existence of excessive torsional rigidity of ribs was not observed to result in significant improvement of the ultimate strength of the stiffened plates.

(3) Except for Case 0, which corresponds to an unstiffened plate, the postbuckling reservation was not found to exist.

(4) The ultimate strength of the tested specimens were well predicted by the formula which one of the authors established for compressed longitudinally stiffened plates without substantial torsional rigidity.

(5) The continuity of the ribs was found quite important since the strength of stiffened plates is significantly depending on whether the ribs are directly loaded or not.

(6) The test rig consisting of universal joints, attachments, and shafts served fairly well to represent the condition of simply supported unloaded edges. However, this rig was observed not sufficient for large deformations of test specimens. Thus, the experimental investigation which takes into account the large displacements in the final stage of loading is strongly recommended. The test specimens should be conveniently of box cross section.

(7) Theoretical analysis was limited to the elastic eigen value analysis. Further researches on the identification of the catastrophic pattern of the buckling and the imperfection sensitivity are highly recommended before going to the nonlinear large deflection analysis combined with elasto-plastic analysis.

7. ACKNOWLEDGEMENT

The authors wish to express appreciation to Mr. M. Yokotsuka of Kashima Construction Company for his assistance in the theoretical and experimental studies.

The study was made possible with the financial support from Sumitomo Metal Industries, Ltd. Especially, the authors would like to extend the appreciation to Mr. H. Inoue of the company for the promotion of the study.

The experimental work was conducted in the Department of Civil Engineering and the Engineering Research Institute of Kyoto University.

The numerical computations were performed mainly by M-190 at Data Processing Center of Kyoto University.

BIBLIOGRAPHY

1) Timoshenko, S. P. and J. M. Gere: Theory of Elastic Stability, McGraw-Hill, New York, 1961.
2) DIN 4114 Blatt 1: Stahlbau, Stabilitätsfälle (Knickung, Kippung, Beulung), Berechnungsgrundlagen, Vorshriften, 1952.
DIN 4114 Blatt 2: Stahlbau, Stabilitätsfälle (Knickung, Kippung, Beulung), Berechnungsgrundlagen, Richtlinien, 1953.
3) Klöppel und Sheer: Beulwerte ausgesteifter Rechteckplatten, W. Ernst und Sohn, 1960.
4) Klöppel und Möller: Beulwerte ausgesteifter Rechteckplatten II, W. Ernst und Sohn, 1968.
5) Wah, T.: Buckling of longitudinally stiffened plates, Aeronautical Quarterly, Vol. 18, pp. 85–99, 1967.
6) Usami, T.: Elastic and inelastic buckling strength of stiffened plates in compression, Proc. JSCE, No. 228, pp. 13–28, 1974.
7) Hasegawa, A., K. Ota, and F. Nishino: Some considerations on buckling of stiffened plates, Proc. JSCE, No. 232, pp. 1–15, 1974.
8) Hasegawa, A., M. Nagahama, and F. Nishino: Buckling strength of stiffened plates under compression, Proc. JSCE, No. 236, pp. 1–14, 1975.
9) Ohmura, H. and Y. Yoshinami: The effects of eccentricity and torsional rigidity of longitudinal stiffeners on the buckling of stiffened plates, Proc. JSCE, pp. 9–15, 1977.
10) Fukumoto, Y., T. Usami, and Y. Okamoto: Ultimate compressive strength of stiffened plates, ASCE Speciality Conference on Metal Bridges, St Louis, 1974.
11) Yamada, Y., E. Watanabe, and M. Yokotsuka: Simplified element method for the analysis of thin plates, Annual Conference of Kansai-District, JSCE, 1976.
12) Nishigomi, A., Y. Niwa, and E. Watanabe: Study on the simplification of structural analysis, Annual Conference of Kansai-District, JSCE 1977.
13) Tateishi, A., Y. Niwa, and E. Watanabe: Application of condensation technique in geometrically nonlinear problems, Annual Conference of Kansai-District, JSCE, 1978.
14) Kawai, T.: New element models in discrete

structural analysis, Annual Conference of Naval Architecture and Shipbuilding in Japan, 1977.

15) Yamada, Y. and E. Watanabe: On the behaviour and ultimate strength of longitudinally stiffened flanges of steel box girders, Proc. JSCE, No. 252, pp. 127–142, 1976.

(*Received December 13, 1977*)